

Article

On the Diffusion of Ionic Liquids in ILs@ZIF-8 Composite Materials: A Density Functional Theory Study

Longlong Liu ¹, Kun Jiang ¹, Qingjun Chen ² and Lei Liu ^{1,*} 

¹ Center for Computational Chemistry, College of Chemistry and Chemical Engineering, Wuhan Textile University, Wuhan 430200, China; 2115383125@mail.wtu.edu.cn (L.L.)

² Key Laboratory of Rare Earths, Ganjiang Innovation Academy, Chinese Academy of Sciences, Ganzhou 341000, China

* Correspondence: liulei3039@gmail.com or liulei@wtu.edu.cn

Abstract: Recently, composite materials consisting of ionic liquids (ILs) and metal–organic frameworks (MOFs) have attracted a great deal of attention due to their fantastic properties. Many theoretical studies have been performed on their special structures and gas separation applications. Yet, the mechanism for the diffusion of ILs inside MOF channels still remains unclear. Here, the DFT calculations (e.g., rigid and relaxed potential energy surface, PES, scan) together with frontier orbital analysis, natural charge analysis, and energy decomposition analysis were performed to investigate the diffusion behavior of a typical IL, [C₄mim][PF₆], into the ZIF-8 SOD cage. The PES profiles indicate that it is quite difficult for the cation [C₄mim]⁺ to diffuse into the cage of ZIF-8 through the pristine pores because of the large imidazole steric hindrance, which results in a large energy barrier of ca. 40 kcal·mol^{−1} at the least. Interestingly, the PES reveals that a successful diffusion could be obtained by thermal contributions, which enlarge the pore size through swing effects at higher temperatures. For example, both [C₄mim]⁺ and [PF₆][−] could easily diffuse through the channel of the ZIF-8 SOD cage when the pore size was increased to 6.9 Å. Subsequently, electronic structure analyses reveal that the main interactions between [PF₆][−] or [C₄mim]⁺ and ZIF-8 are the steric repulsion interactions. Finally, the effects of the amounts of [C₄mim][PF₆] on the ZIF-8 structures were investigated, and the results show that two pairs of [C₄mim][PF₆] per SOD cage are the most stable in terms of the interaction between energies and structural changes. With these findings, we propose that the high-temperature technique could be employed during the synthesis of IL@MOF membranes, to enrich their family members and their industrial applications.

Keywords: ionic liquids; ZIF-8; density functional theory



Citation: Liu, L.; Jiang, K.; Chen, Q.; Liu, L. On the Diffusion of Ionic Liquids in ILs@ZIF-8 Composite Materials: A Density Functional Theory Study. *Molecules* **2024**, *29*, 1697. <https://doi.org/10.3390/molecules29081697>

Academic Editors: Aleksandr S. Kazachenko and Noureddine Issaoui

Received: 27 February 2024

Revised: 1 April 2024

Accepted: 3 April 2024

Published: 9 April 2024



Copyright: © 2024 by the authors. Licensee MDPI, Basel, Switzerland. This article is an open access article distributed under the terms and conditions of the Creative Commons Attribution (CC BY) license (<https://creativecommons.org/licenses/by/4.0/>).

1. Introduction

Recently, composite materials consisting of ionic liquids (ILs) and metal–organic frameworks (MOFs) have attracted considerable attention because of their exceptional properties [1,2]; therefore, they have been used in many important fields, e.g., gas adsorption and separation, catalysis, and sensors [3–13]. In particular, the large number of adsorption sites of MOFs together with ILs play an important role in the gas mixture separation (e.g., CO₂/CH₄) [14–17]. For example, Ban et al. [18] loaded [C₄mim][TF₂N] into the cages of ZIF-8, and the results showed the adsorption selectivity for CO₂/CH₄ significantly increased from 7.5 to 41. Following this work, Kinik et al. [19] examined the [C₄mim][PF₆]/ZIF-8 system via the density functional theory (DFT) and Monte Carlo (MC) simulations. The authors found that the interactions between [C₄mim][PF₆] and ZIF-8 created certain new adsorption sites, which increases the ideal selectivity for CO₂/N₂ from 7.82 to 24.21. Burak et al. [20] obtained a similar result by incorporating [C₄mim][BF₄] into ZIF-8, of which the selectivity of 13.3 has been obtained for CO₂/N₂. Afterwards, a large number of systems have been reported with different combinations of ILs and MOFs [21].

In general, the reasons for ILs@MOFs composite materials with high gas separation or selectivity have been attributed to two main aspects. On the one hand, the rich hydrogen bond network of ILs [22,23] could effectively dissolve CO₂ molecules against other gases, e.g., CH₄ or N₂ [24]; hence, this improves the separation performance compared to pure MOF materials [25–27]. For example, Thomas et al. [28] performed DFT and Giant Canonical Monte Carlo (GCMC) simulations to investigate the selectivity of a series of IL@ZIF-8 systems. Their findings revealed that the hydrophobic fluorinated anions (e.g., [BF₄][−], [Tf₂N][−], and [PF₆][−]) exhibited higher selectivity compared to hydrophilic non-fluorinated anions (e.g., [NO₂][−], [NO₃][−], and [SCN][−]). Kavak et al. [29] investigated the CO₂ separation efficiency of five different IL-encapsulated MIL-53 systems, and they found that the CO₂/CH₄ separation selectivity of [C₄mim][PF₆]/MIL-53 was 2.8 times higher compared to the pure MIL-53. Zhang et al. [30] conducted an investigation on ILs with three different cation functional groups, and the authors revealed that ILs containing amino functional groups exhibited the highest CO₂ molecule affinity and CO₂/CH₄ adsorption selectivity.

On the other hand, it is believed that the introduction of ILs could also modify the structures of the MOFs, and subsequently increase the gas selectivity. Based on the experimental techniques (e.g., high-pressure X-ray diffraction, XRD) with molecular simulations, Fairen et al. [31] demonstrated that the imidazolate linker of the ZIF-8 changed because of the swing effects, and subsequently changed the gas selectivity [32]. Uzun and colleagues [33] coated 1-(2-hydroxyethyl)-3-methylimidazolium dicyanamide ([Hemim][DCA]) on the ZIF-8 surface to eliminate the nonselective voids, and the authors found that the CO₂ selectivity was increased by 45 times compared to the pure ZIF-8. Chang et al. [34] successfully constructed a zwitterionic MOF material (MOF UiO-66-SO₃[−]-NH₃⁺), and the adsorption capacity for CO₂ increased by 32–48%, because the positive and negative charges on the modified MOF material interacted with the ILs of [Emim][SCN]. Our previous theoretical studies [35,36] revealed that the ZIF-8 aperture configurations have a significant impact on the separation of CO₂/CH₄. Specifically speaking, the DFT calculations showed that the pristine ZIF-8 aperture (with a pore size of 3.4 Å) exhibits the best separation performance, which has the largest energy barrier difference between CO₂ and CH₄; additionally, the MD simulations revealed that ILs (e.g., [C₄mim][PF₆]) could effectively maintain pristine aperture configurations, and retained the high separation properties.

Yet, there are still open questions following the reported mechanistic studies; that is to say, how do the ILs diffuse into the cage of MOFs (e.g., ZIF-8)? And, how many ILs could be accommodated per cage? In this vein, we performed DFT calculations to investigate the diffusion behavior of ILs into MOF cages by taking [C₄mim][PF₆] and ZIF-8 as an example. Firstly, the potential energy surface (PES) scan was performed to study the passing of [C₄mim]⁺ and [PF₆][−] through different ZIF-8 apertures. Secondly, several electronic analysis methods, including frontier orbital energies, natural charge analysis, and energy decomposition analysis, were used to investigate the interactions between [C₄mim]⁺/[PF₆][−] and ZIF-8. Lastly, a series of IL-encapsulated ZIF-8 with different loading amounts were investigated to obtain stabilities of ionic pairs in the SOD cage of ZIF-8.

2. Results

First of all, we performed the DFT-based PES scan calculations. In general, small energy barriers would indicate a smooth diffusion of ILs inside the pore structures of MOFs. The PES scan of the [C₄mim]⁺ and [PF₆][−] passing through the pristine ZIF-8 aperture (with a pore size of 3.4 Å) is shown in Figure 1a. It is shown that both [C₄mim]⁺ and [PF₆][−] almost cannot pass through the pore because of their large energy barriers. For [C₄mim]⁺, an energy barrier of 135.5 kcal·mol^{−1} was obtained, and the corresponding structure is the one when the COM of imidazole almost perpendicularly overlaps with the COM of the pristine ZIF-8 aperture. For [PF₆][−], three cases have been considered (see Materials and Methods (Section 3)). The lowest energy barrier, which is 69.17 kcal·mol^{−1}, was found for case III, in which three F atoms pointed to the plane of the ZIF-8 apertures. This finding could be explained by their molecular diameters, in which case I has a diameter of 3.29 Å, case II

has a diameter of 3.20 Å, and case **III** has a diameter of 2.94 Å (Figure S1). Meanwhile, as shown in Figure S2, the results of the energy decomposition analysis show that the repulsive interactions between the $[\text{PF}_6]^-$ and ZIF-8 are the smallest when $[\text{PF}_6]^-$ adopted case **III**. After obtaining the configurations with the highest energy barriers, we then refined the PES with the relaxed scan (see Figure 1b), and we found that both $[\text{C}_4\text{mim}]^+$ and $[\text{PF}_6]^-$ still have relatively high energy barriers, being $39.87 \text{ kcal}\cdot\text{mol}^{-1}$ and $16.61 \text{ kcal}\cdot\text{mol}^{-1}$, respectively, which still prohibited $[\text{C}_4\text{mim}]^+$ and $[\text{PF}_6]^-$ from diffusing into the SOD cage of ZIF-8 at finite temperatures, e.g., room temperature. In detail, only one energy barrier was found when $[\text{PF}_6]^-$ moved from the left to the right side of the pore, and the highest energy point corresponds to the structure of which the P atom is located at the plane of the pristine ZIF-8, with three F atoms located at each side (see Figure S3a). The average distance between the H atoms of ZIF-8 and the F atoms of the $[\text{PF}_6]^-$ is computed to be 2.52 Å. While for the $[\text{C}_4\text{mim}]^+$, two energy barriers were found when $[\text{C}_4\text{mim}]^+$ moved from the left to the right of the pristine ZIF-8 aperture. The first one, $14.60 \text{ kcal}\cdot\text{mol}^{-1}$, corresponds to the passing of the alkyl chain, in which the average distance between the alkyl chain and the ZIF-8 aperture is 2.61 Å. The second one, $39.87 \text{ kcal}\cdot\text{mol}^{-1}$, corresponds to the passing of the imidazole ring, in which the average distance between the imidazole ring and the ZIF-8 aperture is only 1.66 Å (Figure S3b); hence, such small distances result in large steric hindrances or strong repulsion interactions.

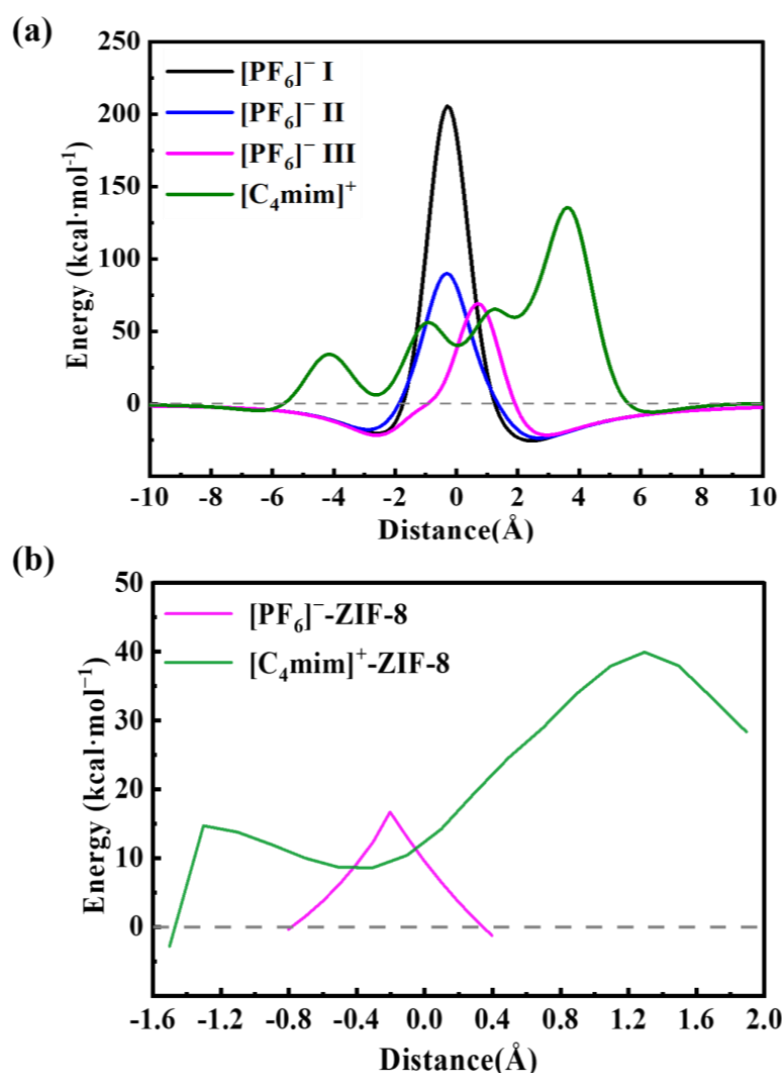


Figure 1. The potential energy surface curves for the anion $[\text{PF}_6]^-$ and cation $[\text{C}_4\text{mim}]^+$ passing through ZIF-8 structures: (a) the rigid PES scan and (b) the relaxed PES scan.

Afterwards, the frontier orbitals, including the highest occupied molecular orbital (HOMO) and the lowest unoccupied molecular orbital (LUMO) were plotted in Figure 2. In general, the results indicate that there are no significant orbital interactions between the $[\text{C}_4\text{mim}]^+ / [\text{PF}_6]^-$ and the pristine ZIF-8 aperture within the frontier orbital scheme. For example, both the LUMOs and HOMOs of $[\text{C}_4\text{mim}]^+ \text{-ZIF-8}$ and $[\text{PF}_6]^- \text{-ZIF-8}$ are almost the same compared to those of the free pristine ZIF-8 aperture; in other words, the frontier orbitals mainly consist of the contributions from the ZIF-8 aperture. The HOMO–LUMO gaps of $[\text{C}_4\text{mim}]^+ \text{-ZIF-8}$ and $[\text{PF}_6]^- \text{-ZIF-8}$ are also identical to those of the free pristine ZIF-8 aperture, e.g., 0.64 eV versus 0.65 eV. Moreover, the natural population analysis (NPA) was performed, and the natural charges as summarized in Table S1. The values show that a certain number of charges (ca. 0.08 e) have been transferred between $[\text{C}_4\text{mim}]^+$ and $[\text{PF}_6]^-$ and the pristine ZIF-8 apertures.

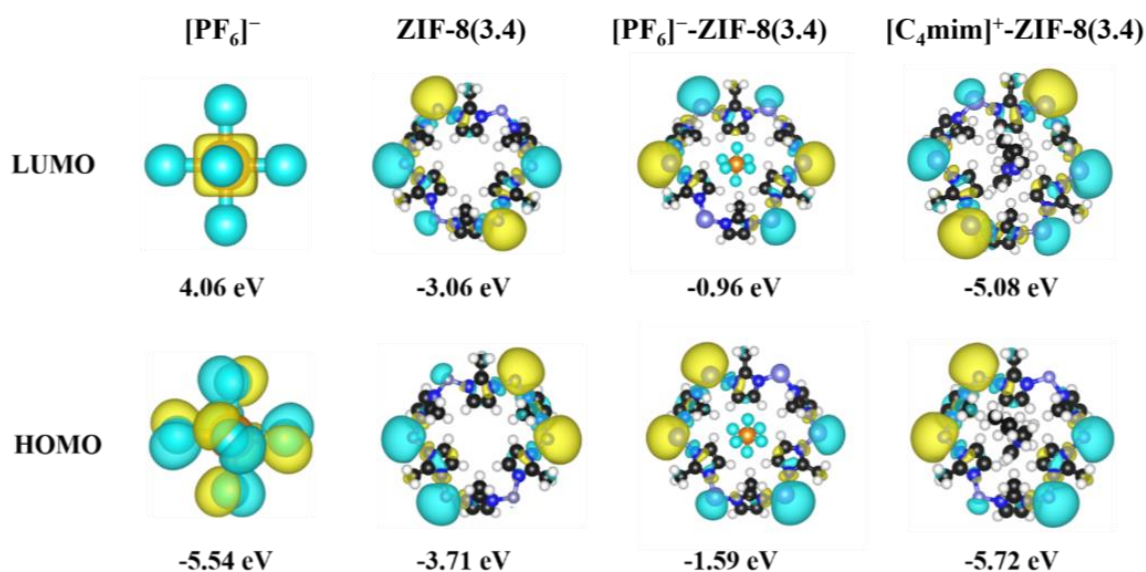


Figure 2. Frontier orbitals and their energies, with an isosurface value of $0.05 \text{ e}/\text{\AA}^3$.

To have a deep understanding of the interactions between $[\text{C}_4\text{mim}]^+ / [\text{PF}_6]^-$ and the pristine ZIF-8 aperture, the GKS-EDA energy decomposition analysis has been performed based on the $[\text{PF}_6]^- \text{-ZIF-8(3.4 \text{ \AA})}$ and $[\text{C}_4\text{mim}]^+ \text{-ZIF-8(3.4 \text{ \AA})}$ structures and the results are plotted in Figure 3. Generally, the interaction energies are decomposed according to the following equations:

$$\Delta E^{total} = \Delta E^{ex} + \Delta E^{rep} + \Delta E^{corr} + \Delta E^{ele} + \Delta E^{pol} + \Delta E^{disp},$$

where ΔE^{ex} , ΔE^{rep} , ΔE^{corr} , ΔE^{ele} , ΔE^{pol} , and ΔE^{disp} represent exchange, repulsion, correlation, electrostatic, polarization, and dispersion components, respectively. As shown in Figure 3, the interaction energies are dominated by three terms, including the repulsion, exchange, and electrostatic energies, of which the repulsions are the main reason for the high energy barriers shown in Figure 1. The rest of the components are relatively small (e.g., less than $28 \text{ kcal}\cdot\text{mol}^{-1}$ in absolute values, and with a total ratio being less than 6.6%). Here, we take $[\text{C}_4\text{mim}]^+ \text{-ZIF-8(3.4 \text{ \AA})}$ as an example and discuss those three terms individually: (1) The repulsion component. This term is responsible for steric repulsion, and it consists of the destabilizing interactions between occupied orbitals of the fragments. Usually, this term is repulsive (with a positive computed value). Here, a value of $304.27 \text{ kcal}\cdot\text{mol}^{-1}$ was obtained, which can be attributed to the large steric repulsion between the imidazole ring of $[\text{C}_4\text{mim}]^+$ and the pristine ZIF-8 aperture. As discussed in the PES scan section, the pristine ZIF-8 aperture has a pore size of only 3.4 \AA ; hence, this leaves the imidazole ring few spaces to pass through. (2) The exchange component. This term essentially is related to

electrons with the same spin, exchanging their positions in degenerate orbitals to increase the stability of electronic structure states. Here, we found a value of $-162.2 \text{ kcal}\cdot\text{mol}^{-1}$, in the case of $[\text{C}_4\text{mim}]^+\text{-ZIF-8}$. (3) The electrostatic component. This term is the energy between the unperturbed charge distributions of the prepared fragments, which is usually attractive. As shown in Figure 3, the computed electrostatic interaction is $-50 \text{ kcal}\cdot\text{mol}^{-1}$, which is much smaller compared to the repulsion and exchange interactions. This finding is somehow consistent with the NPA charge analysis, in which the pristine ZIF-8 is slightly charged (ca. $0.08 e$) via the charge transfer from $[\text{C}_4\text{mim}]^+$.

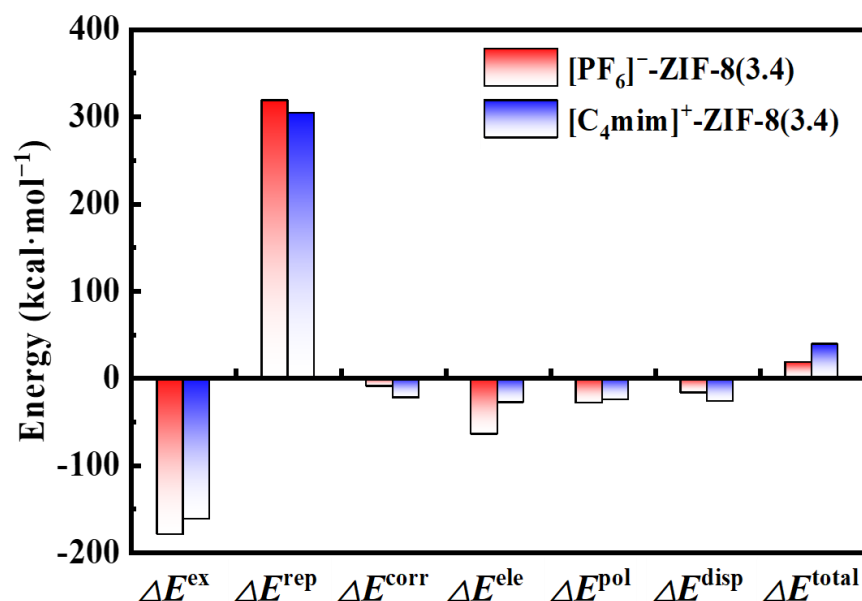


Figure 3. Energy decomposition analysis calculated with the GKS-EDA method at the B3LYP-D3(BJ)/6-311+G* level of theory for the $[\text{PF}_6]^- / [\text{C}_4\text{mim}]^+ \text{-ZIF-8(3.4)}$ systems.

Our previous MD simulations showed that the pristine ZIF-8 aperture could be distorted because of the thermal oscillations [36]. When the simulations were performed at a temperature of 300 K, an average of 6.8 Å movements was obtained for the atoms defined by the size and shape of the pores. In other words, we could conclude that the ZIF-8 structure is very flexible against the temperatures, and the pore size might be modified by varying the synthesis temperatures. Following that study, here, we computed the PES scan of $[\text{C}_4\text{mim}]^+$ and $[\text{PF}_6]^-$ passing through the ZIF-8 aperture with the pore size of 4.1 Å, 4.2 Å, 4.7 Å, and 6.9 Å, respectively, (the pore structures are depicted in Materials and Methods (Section 3)), and the results are summarized in Figure 4. Generally, the results show that the $[\text{PF}_6]^-$ is able to freely pass through these pores with energy barriers under zero. However, $[\text{C}_4\text{mim}]^+$ can only pass through the pore with a diameter of 6.9 Å. Together with our previous room-temperature MD simulations, we conclude that a higher temperature might be needed to obtain a larger swing effect and to encapsulate $[\text{C}_4\text{mim}][\text{PF}_6]$ into the ZIF-8 SOD cage. These findings are rather qualitatively consistent with a reported experiment study, in which the authors employed a two-step adsorption/infiltration method to incorporate $[\text{C}_4\text{mim}][\text{PF}_6]$ into ZIF-8 [37]. In that work, $[\text{C}_4\text{mim}][\text{PF}_6]$ were firstly adsorbed on the outer surface of ZIF-8, then through heat treatment at 105 °C, $[\text{C}_4\text{mim}][\text{PF}_6]$ molecules infiltrated into the SOD cage. Afterwards, the temperature was cooled down to room temperature, and then the $[\text{C}_4\text{mim}][\text{PF}_6]$ -encapsulated ZIF-8 composite materials were obtained.

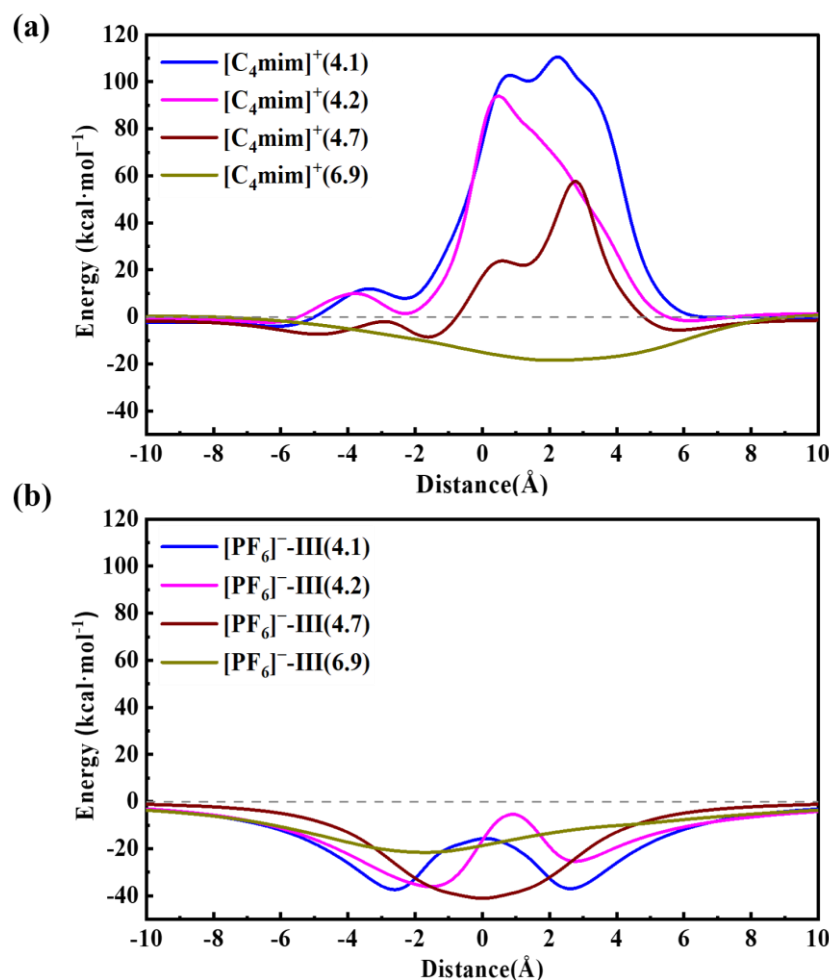


Figure 4. Potential energy surface curves for $[\text{C}_4\text{mim}]^+$ (a) and $[\text{PF}_6]^-$ (b) passing through different ZIF-8 apertures.

Lastly, to study how many pairs of $[\text{C}_4\text{mim}][\text{PF}_6]$ could be stable inside the ZIF-8 SOD cage, and to examine the impact of their contents on the structures of the ZIF-8 apertures, the structural optimizations were performed by adding one, two, and three pairs of $[\text{PF}_6][\text{C}_4\text{mim}]$ in the pristine ZIF-8 SOD cage. As shown in Figure 5a, it is shown that the interaction energies between $[\text{C}_4\text{mim}][\text{PF}_6]$ and ZIF-8 were strongest when two pairs of $[\text{C}_4\text{mim}][\text{PF}_6]$ were added, with a computed value of $-44.81 \text{ kcal}\cdot\text{mol}^{-1}$, whereas the interactions energies of one and three pairs were computed to be $-35.69 \text{ kcal}\cdot\text{mol}^{-1}$ and $-40.92 \text{ kcal}\cdot\text{mol}^{-1}$. As such, we conclude that most of the ZIF-8 SOD cages could accommodate two pairs of $[\text{C}_4\text{mim}][\text{PF}_6]$, and some of them are even able to accommodate three pairs. Overall, a value slightly larger than 2 would be obtained for the pairs of $[\text{C}_4\text{mim}][\text{PF}_6]$ per SOD cage. These findings are comparable to the experimental results obtained by Ban et al. [18], in which an average of 1.4 pairs of $[\text{C}_4\text{mim}][\text{TF}_2\text{N}]$ was identified per ZIF-8 SOD cage. The smaller value of 1.4 versus 2.0 could be attributed to the fact that the anion $[\text{TF}_2\text{N}]^-$ is relatively larger than $[\text{PF}_6]^-$ in space size. Compared to the experimental values [38], we found that the volume of the ZIF-8 SOD cage was increased when $[\text{C}_4\text{mim}][\text{PF}_6]$ was encapsulated, of which the smallest value was obtained (0.9%) for the case with two pairs. Moreover, we also observed certain confinement effects from the results shown in Figure 5c, e.g., the structure of one pair of $[\text{C}_4\text{mim}][\text{PF}_6]$ is very similar compared to the free pair (e.g., gas phase calculations), while the two and three pairs show structures closer to the condensed phase [39].

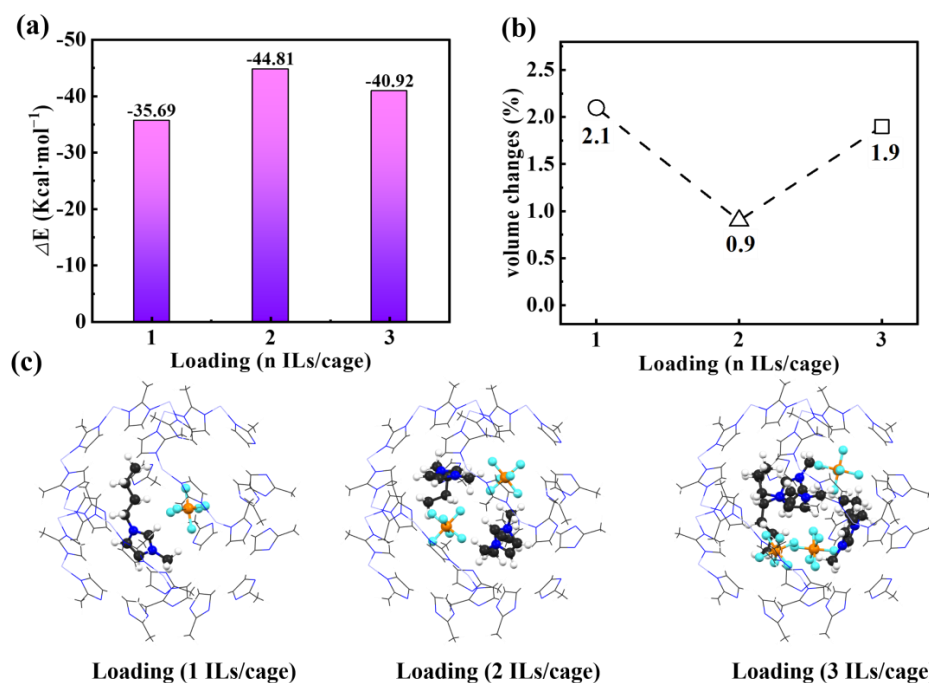


Figure 5. Interaction energies (a), volume changes (b), and geometric structures (c) of the ZIF-8 SOD cage containing one, two, and three pairs of $[\text{PF}_6][\text{C}_4\text{mim}]$, respectively.

3. Materials and Methods

The crystal structure of the ZIF-8 was obtained from the Cambridge Crystallographic Data Centre (CCDC) Crystal Library [24], and the simplified SOD cage presentation is depicted in Figure 6a. We choose the five typical pore apertures of the ZIF-8 structure as the result of the rotation of the zinc–imidazole–zinc and methyl functional groups, as described by our previous work, [35], including “Pristine (3.4 Å)”, “Closed” (4.1 Å), “Semi-open (4.2 Å)”, “Closed (4.7 Å)”, and “Open” (6.9 Å), respectively, which are shown in Figure 6b–f.

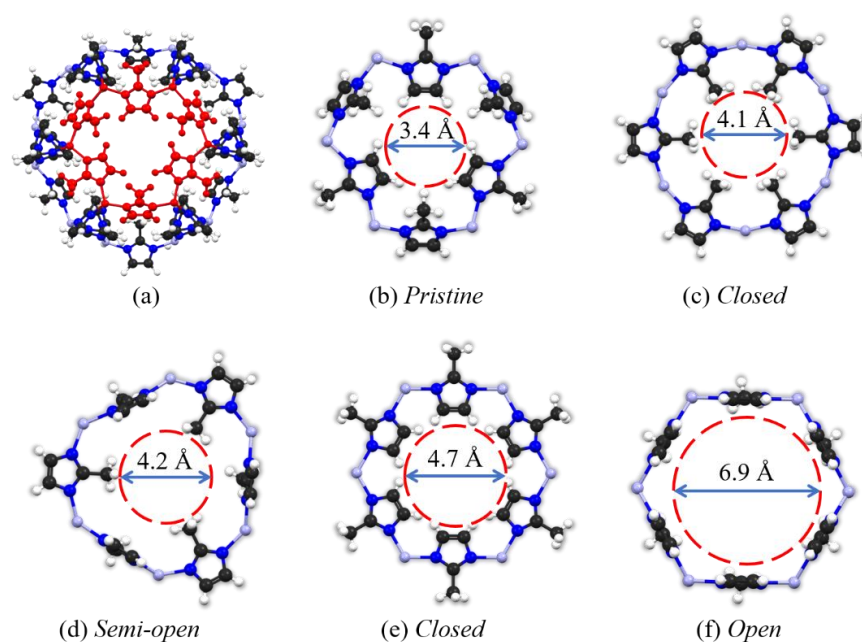


Figure 6. (a) The SOD cage presentation of the ZIF-8, and its typical (pristine) pore structure is highlighted in red color; (b–f) five different pore structures of ZIF-8 with their diameters (ref. [33]). Color legend: C, black; N, blue; Zn, light grey; H, white.

As demonstrated in Figure 7a, the $[\text{PF}_6]^-$ and $[\text{C}_4\text{mim}]^+$ were firstly placed 10 Å away from the aperture of the ZIF-8; then, gradually (e.g., with a step size of 0.1 Å), penetrate passed through the center of the aperture (the center of mass, COM). In principle, $[\text{PF}_6]^-$ and $[\text{C}_4\text{mim}]^+$ might have many orientations when passing through the five pore structures as shown in Figure 6. Here, we considered only the orientations that have possible low energy barriers. To summarize Figure 7b, three different orientations of $[\text{PF}_6]^-$ have been studied, denoted as case I, II, and III, with one, two, and three fluorine atoms (F) towards the aperture, respectively. For the $[\text{C}_4\text{mim}]^+$, one case was chosen towards the aperture, of which the imidazole ring is almost vertical to the aperture.

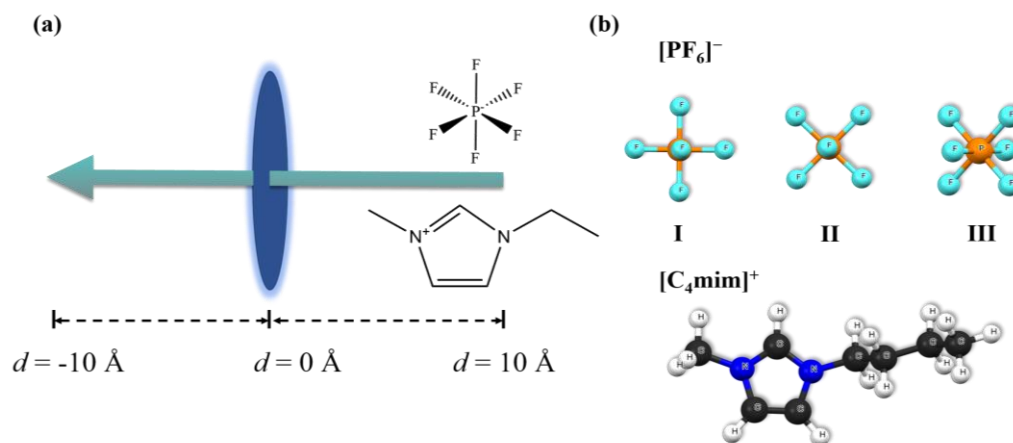


Figure 7. (a) Schematic representation of $[\text{PF}_6]^-/[\text{C}_4\text{mim}]^+$ passing through ZIF-8 apertures. (b) The geometric structures of $[\text{PF}_6]^-/[\text{C}_4\text{mim}]^+$, and their orientations when passing through the ZIF-8 aperture.

With the above-described models, rigid PES scans with single-point (SP) energy calculations were performed, where all atoms in the aperture of ZIF-8 and $[\text{PF}_6]^-/[\text{C}_4\text{mim}]^+$ were kept frozen. Afterward, we performed the relaxed PES scan within the regions near the highest energy barrier positions from the rigid PES scans (e.g., ca. -2 Å to 2 Å). In these cases, the atoms in the aperture of ZIF-8 were kept frozen, while $[\text{PF}_6]^-/[\text{C}_4\text{mim}]^+$ were fully optimized. Both PES scans were carried out with the Gaussian16 software package [40]. In the next discussion of both rigid and relaxed PES scans, we mainly focus on the largest energy barriers, which are the energy differences between the highest point on the PES and the free IL plus ZIF-8 structures. Subsequently, the orbital energies and charge transfer were computed with natural population analysis (NPA) [41] using the Multiwfn v.3.7 [42] software package and visualized using the VESTA v.3.5.8 [43] software package. To quantitatively study the interactions between $[\text{PF}_6]^-/[\text{C}_4\text{mim}]^+$ and ZIF-8, the energy decomposition analysis was performed based on the generalized Kohn–Sham energy density analysis (GKS-EDA) method [44], which is implemented in the GAMESS program package [45]. All above-mentioned DFT calculations were performed at the B3LYP level of theory, with a basis set of 6-311+G* [46], together with the damping scheme of Becke and Johnson, which denoted as DFT-D3 (BJ) [47,48].

Lastly, to study how many pairs are stable inside the SOD cage of ZIF-8, the periodic structures of ILs@ZIF-8 were examined by the BLYP functional with the dispersion correction scheme (DFT-D3). The geometry optimizations were performed to account for both changes in atomic positions and lattice dimensions, which were updated with the efficient L-BFGS algorithm. Within the DFT calculations, the DZVP-MOLOPT-SR-GTH basis set was adopted for Zn atoms, while the other atoms used the TZVP-MOLOPT -GTH basis set. The energy cutoff was set to 400 Ry, and the energy convergence for the self-consistent field (SCF) calculation was set to 1×10^{-5} Hartree. All those periodic calculations were performed by employing the CP2K's Quickstep module [49].

4. Conclusions

In summary, the DFT calculations and several electronic structure analyses have been performed to study the diffusion behavior of the ILs, $[\text{C}_4\text{mim}][\text{PF}_6]$, through the different aperture configurations of ZIF-8, and their stabilities inside the ZIF-8 cage. The results indicate that the original aperture configuration (with a 3.4 Å pore size) eventually prohibits the diffusion of $[\text{C}_4\text{mim}][\text{PF}_6]$ into the SOD cage of ZIF-8, as a minimum energy barrier of $39.87 \text{ kcal}\cdot\text{mol}^{-1}$ had been identified, which is mainly due to steric hindrance from the imidazole ring of the $[\text{C}_4\text{mim}]^+$. The energy decomposition analysis based on the GKS-EDA method revealed that the large repulsion component is the main reason for the high energy barriers when $[\text{C}_4\text{mim}]^+$ and $[\text{PF}_6]^-$ pass through the pristine ZIF-8 aperture. Nevertheless, we found that the diffusion properties could be largely enhanced by modifying the ZIF-8 apertures, e.g., the pore size, and it is proved that this could be achieved via thermal contributions (e.g., employing a higher temperature during the synthesis procedure). Moreover, we found that two pairs of $[\text{C}_4\text{mim}][\text{PF}_6]$ per SOD cage is the stable state, according to interaction energies and volume changes. Certain confinement effects were obtained as well, in which the structure of one pair of $[\text{C}_4\text{mim}][\text{PF}_6]$ is similar compared to the free pair, while the two and three pairs show structures closer to the condensed phase.

Supplementary Materials: The following supporting information can be downloaded at <https://www.mdpi.com/article/10.3390/molecules29081697/s1>: Figure S1: Three different ways and their diameters of the $[\text{PF}_6]$ pathing through the ZIF-8 pore; Figure S2: Interaction energy components calculated using the GKS-EDA method at the B3LYP-D3(BJ)/6-311+G* level for the different $[\text{PF}_6]^-$ ways towards the ZIF-8 aperture; Figure S3: The structures for the points with the highest interaction energies in the cases of $[\text{PF}_6]^-/[\text{C}_4\text{mim}]^+$ and ZIF-8(3.4), respectively, and the average distance refers to the closest distances between the fluorine atom on the $[\text{PF}_6]^-$, or the hydrogen atoms on the $[\text{C}_4\text{mim}]^+$ and the hydrogen atom on the aperture; and Table S1: NPA charge analysis of $[\text{PF}_6]^-/[\text{C}_4\text{mim}]^+$ and ZIF-8(3.4) at theoretical levels of B3LYP-D3(BJ)/6-311+G*.(values are in *e*).

Author Contributions: Investigation, L.L. (Longlong Liu) and K.J.; Data Curation, L.L. (Longlong Liu) and K.J.; Writing—Original Draft, L.L. (Longlong Liu) and K.J.; Writing—Review and Editing, Q.C. and L.L. (Lei Liu); Supervision, Q.C. and L.L. (Lei Liu). All authors have read and agreed to the published version of the manuscript.

Funding: L.L. is thankful for the financial support in the form of start-up funding from Wuhan Textile University (No. 20220321).

Institutional Review Board Statement: Not applicable.

Informed Consent Statement: Not applicable.

Data Availability Statement: The original contributions presented in the study are included in the article/Supplementary Materials. Further inquiries can be directed to the corresponding authors.

Conflicts of Interest: The authors declare that they have no known competing financial interests.

References

1. Li, X.; Chen, K.; Guo, R.; Wei, Z. Ionic Liquids Functionalized MOFs for Adsorption. *Chem. Rev.* **2023**, *123*, 10432–10467. [[CrossRef](#)] [[PubMed](#)]
2. Durak, O.; Zeeshan, M.; Habib, N.; Gulbalkan, H.C.; Alshihle, A.A.A.M.; Caglayan, H.P.; Kurtoğlu-Öztulum, S.F.; Zhao, Y.; Haslak, Z.P.; Uzun, A.; et al. Composites of porous materials with ionic liquids: Synthesis, characterization, applications, and beyond. *Microporous Mesoporous Mater.* **2022**, *332*, 111703. [[CrossRef](#)]
3. Wu, K.; Miao, X.; Zhao, H.; Liu, S.; Fei, T.; Zhang, T. Selective Encapsulation of Ionic Liquids in UiO-66-NH₂ Nanopores for Enhanced Humidity Sensing. *ACS Appl. Nano Mater.* **2023**, *6*, 9050–9058. [[CrossRef](#)]
4. Qian, Y.; Zhang, F.; Pang, H. A Review of MOFs and Their Composites-Based Photocatalysts: Synthesis and Applications. *Adv. Funct. Mater.* **2021**, *31*, 2104231. [[CrossRef](#)]
5. Friess, K.; Izák, P.; Kárászová, M.; Pasichnyk, M.; Lanč, M.; Nikolaeva, D.; Luis, P.; Jansen, J.C. A Review on Ionic Liquid Gas Separation Membranes. *Membranes* **2021**, *11*, 97. [[CrossRef](#)] [[PubMed](#)]

6. Fernandez, E.; Saiz, P.G.; Peřinka, N.; Wuttke, S.; Fernández de Luis, R. Printed Capacitive Sensors Based on Ionic Liquid/Metal-Organic Framework Composites for Volatile Organic Compounds Detection. *Adv. Funct. Mater.* **2021**, *31*, 2010703. [[CrossRef](#)]
7. Tuffnell, J.M.; Morzy, J.K.; Kelly, N.D.; Tan, R.; Song, Q.; Ducati, C.; Bennett, T.D.; Dutton, S.E. Comparison of the ionic conductivity properties of microporous and mesoporous MOFs infiltrated with a Na-ion containing IL mixture. *Dalton Trans.* **2020**, *49*, 15914–15924. [[CrossRef](#)]
8. Zeeshan, M.; Nozari, V.; Keskin, S.; Uzun, A. Structural Factors Determining Thermal Stability Limits of Ionic Liquid/MOF Composites: Imidazolium Ionic Liquids Combined with CuBTC and ZIF-8. *Ind. Eng. Chem. Res.* **2019**, *58*, 14124–14138. [[CrossRef](#)]
9. Yoshida, Y.; Fujie, K.; Lim, D.W.; Ikeda, R.; Kitagawa, H. Superionic Conduction over a Wide Temperature Range in a Metal-Organic Framework Impregnated with Ionic Liquids. *Angew. Chem. Int. Ed.* **2019**, *58*, 10909–10913. [[CrossRef](#)] [[PubMed](#)]
10. Li, H.; Tuo, L.; Yang, K.; Jeong, H.-K.; Dai, Y.; He, G.; Zhao, W. Simultaneous enhancement of mechanical properties and CO₂ selectivity of ZIF-8 mixed matrix membranes: Interfacial toughening effect of ionic liquid. *J. Membr. Sci.* **2016**, *511*, 130–142. [[CrossRef](#)]
11. Khan, M.S.; Li, Y.; Yang, L.; Yan, Z.C.; Li, D.-S.; Qiu, J.; Xu, X.; Yang, H.Y. Improving capacitive deionization performance through tailored iodine-loaded ZIF-8 composites. *Desalination* **2024**, *579*, 117486. [[CrossRef](#)]
12. Khan, M.S.; Leong, Z.Y.; Li, D.-S.; Qiu, J.; Xu, X.; Yang, H.Y. A mini review on metal-organic framework-based electrode materials for capacitive deionization. *Nanoscale* **2023**, *15*, 15929–15949. [[CrossRef](#)] [[PubMed](#)]
13. Khan, M.S.; Li, Y.; Li, D.-S.; Qiu, J.; Xu, X.; Yang, H.Y. A review of metal-organic framework (MOF) materials as an effective photocatalyst for degradation of organic pollutants. *Nanoscale Adv.* **2023**, *5*, 6318–6348. [[CrossRef](#)] [[PubMed](#)]
14. Chen, W.; Zhang, Z.; Yang, C.; Liu, J.; Shen, H.; Yang, K.; Wang, Z. PIM-based mixed-matrix membranes containing MOF-801/ionic liquid nanocomposites for enhanced CO₂ separation performance. *J. Membr. Sci.* **2021**, *636*, 119581. [[CrossRef](#)]
15. Zeeshan, M.; Keskin, S.; Uzun, A. Enhancing CO₂/CH₄ and CO₂/N₂ separation performances of ZIF-8 by post-synthesis modification with [BMIM][SCN]. *Polyhedron* **2018**, *155*, 485–492. [[CrossRef](#)]
16. Krokidas, P.; Moncho, S.; Brothers, E.N.; Castier, M.; Economou, I.G. Tailoring the gas separation efficiency of metal organic framework ZIF-8 through metal substitution: A computational study. *Phys. Chem. Chem. Phys.* **2018**, *20*, 4879–4892. [[CrossRef](#)] [[PubMed](#)]
17. Gulbalkan, H.C.; Haslak, Z.P.; Altintas, C.; Uzun, A.; Keskin, S. Assessing CH₄/N₂ separation potential of MOFs, COFs, IL/MOF, MOF/Polymer, and COF/Polymer composites. *Chem. Eng. J.* **2022**, *428*, 131239. [[CrossRef](#)]
18. Ban, Y.; Li, Z.; Li, Y.; Peng, Y.; Jin, H.; Jiao, W.; Guo, A.; Wang, P.; Yang, Q.; Zhong, C.; et al. Confinement of Ionic Liquids in Nanocages: Tailoring the Molecular Sieving Properties of ZIF-8 for Membrane-Based CO₂ Capture. *Angew. Chem. Int. Ed. Engl.* **2015**, *54*, 15483–15487. [[CrossRef](#)] [[PubMed](#)]
19. Kinik, F.P.; Altintas, C.; Balci, V.; Koyuturk, B.; Uzun, A.; Keskin, S. [BMIM][PF6] Incorporation Doubles CO₂ Selectivity of ZIF-8: Elucidation of Interactions and Their Consequences on Performance. *ACS Appl. Mater. Interfaces* **2016**, *8*, 30992–31005. [[CrossRef](#)] [[PubMed](#)]
20. Koyuturk, B.; Altintas, C.; Kinik, F.P.; Keskin, S.; Uzun, A. Improving Gas Separation Performance of ZIF-8 by [BMIM][BF4] Incorporation: Interactions and Their Consequences on Performance. *J. Phys. Chem. C* **2017**, *121*, 10370–10381. [[CrossRef](#)]
21. Ali, S.A.; Khan, A.U.; Mulk, W.U.; Khan, H.; Nasir Shah, S.; Zahid, A.; Habib, K.; Shah, M.U.H.; Othman, M.H.D.; Rahman, S. An Ongoing Futuristic Career of Metal-Organic Frameworks and Ionic Liquids, A Magical Gateway to Capture CO₂; A Critical Review. *Energy Fuels* **2023**, *37*, 15394–15428. [[CrossRef](#)]
22. Dong, K.; Liu, X.; Dong, H.; Zhang, X.; Zhang, S. Multiscale Studies on Ionic Liquids. *Chem. Rev.* **2017**, *117*, 6636–6695. [[CrossRef](#)] [[PubMed](#)]
23. Chen, J.; Dong, K.; Liu, L.; Zhang, X.; Zhang, S. Anti-electrostatic hydrogen bonding between anions of ionic liquids: A density functional theory study. *Phys. Chem. Chem. Phys.* **2021**, *23*, 7426–7433. [[CrossRef](#)] [[PubMed](#)]
24. Kwon, H.T.; Jeong, H.-K.; Lee, A.S.; An, H.S.; Lee, J.S. Heteroepitaxially Grown Zeolitic Imidazolate Framework Membranes with Unprecedented Propylene/Propane Separation Performances. *J. Am. Chem. Soc.* **2015**, *137*, 12304–12311. [[CrossRef](#)] [[PubMed](#)]
25. Thomas, A.; Prakash, M. Tuning the CO₂ adsorption by the selection of suitable ionic liquids at ZIF-8 confinement: A DFT study. *Appl. Surf. Sci.* **2019**, *491*, 633–639. [[CrossRef](#)]
26. Mohamed, A.M.O.; Moncho, S.; Krokidas, P.; Kakosimos, K.; Brothers, E.N.; Economou, I.G. Computational investigation of the performance of ZIF-8 with encapsulated ionic liquids towards CO₂ capture. *Mol. Phys.* **2019**, *117*, 3791–3805. [[CrossRef](#)]
27. Gao, W.; Zheng, W.; Sun, W.; Zhao, L. Understanding the Effective Capture of H₂S/CO₂ from Natural Gas Using Ionic Liquid@MOF Composites. *J. Phys. Chem. C* **2022**, *126*, 19872–19882. [[CrossRef](#)]
28. Thomas, A.; Ahamed, R.; Prakash, M. Selection of a suitable ZIF-8/ionic liquid (IL) based composite for selective CO₂ capture: The role of anions at the interface. *RSC Adv.* **2020**, *10*, 39160–39170. [[CrossRef](#)] [[PubMed](#)]
29. Kavak, S.; Polat, H.M.; Kulak, H.; Keskin, S.; Uzun, A. MIL-53(Al) as a Versatile Platform for Ionic-Liquid/MOF Composites to Enhance CO₂ Selectivity over CH₄ and N₂. *Chem.-Asian J.* **2019**, *14*, 3655–3667. [[CrossRef](#)] [[PubMed](#)]
30. Zhang, Z.; Jia, X.; Sun, Y.; Guo, X.; Huang, H.; Zhong, C. Pore engineering of ZIF-8 with ionic liquids for membrane-based CO₂ separation: Bearing functional group effect. *Green Chem. Eng.* **2021**, *2*, 104–110. [[CrossRef](#)]
31. Fairen-Jimenez, D.; Moggach, S.A.; Wharmby, M.T.; Wright, P.A.; Parsons, S.; Düren, T. Opening the Gate: Framework Flexibility in ZIF-8 Explored by Experiments and Simulations. *J. Am. Chem. Soc.* **2011**, *133*, 8900–8902. [[CrossRef](#)] [[PubMed](#)]

32. Zhang, C.; Lively, R.P.; Zhang, K.; Johnson, J.R.; Karvan, O.; Koros, W.J. Unexpected Molecular Sieving Properties of Zeolitic Imidazolate Framework-8. *J. Phys. Chem. Lett.* **2012**, *3*, 2130–2134. [[CrossRef](#)] [[PubMed](#)]
33. Zeeshan, M.; Nozari, V.; Yagci, M.B.; Isik, T.; Unal, U.; Ortalan, V.; Keskin, S.; Uzun, A. Core–Shell Type Ionic Liquid/Metal Organic Framework Composite: An Exceptionally High CO₂/CH₄ Selectivity. *J. Am. Chem. Soc.* **2018**, *140*, 10113–10116. [[CrossRef](#)]
34. Chang, Y.; Wang, L.; Jiang, Z.; Zhang, R.; Zhu, H.; Zhang, D.; Zhu, J.; Kong, X.; Huang, H. Zwitterionic metal–organic framework with highly dispersed ionic liquid for enhancing CO₂ capture. *Sep. Purif. Technol.* **2023**, *326*, 124828. [[CrossRef](#)]
35. Yu, T.; Cai, Q.; Lian, G.; Bai, Y.; Zhang, X.; Zhang, X.; Liu, L.; Zhang, S. Mechanisms behind high CO₂/CH₄ selectivity using ZIF-8 metal organic frameworks with encapsulated ionic liquids: A computational study. *Chem. Eng. J.* **2021**, *419*, 129638. [[CrossRef](#)]
36. Yu, T.; Cai, Q.; Lian, G.; Liu, L. Molecular dynamics studies on separation of CO₂/CH₄ by the ionic liquids encapsulated ZIF-8. *J. Membr. Sci.* **2022**, *644*, 120117. [[CrossRef](#)]
37. Guo, Z.; Zheng, W.; Yan, X.; Dai, Y.; Ruan, X.; Yang, X.; Li, X.; Zhang, N.; He, G. Ionic liquid tuning nanocage size of MOFs through a two-step adsorption/infiltration strategy for enhanced gas screening of mixed-matrix membranes. *J. Membr. Sci.* **2020**, *605*, 118101. [[CrossRef](#)]
38. Park, K.S.; Ni, Z.; Côté, A.P.; Choi, J.Y.; Huang, R.; Uribe-Romo, F.J.; Chae, H.K.; O’Keeffe, M.; Yaghi, O.M. Exceptional chemical and thermal stability of zeolitic imidazolate frameworks. *Proc. Natl. Acad. Sci. USA* **2006**, *103*, 10186–10191. [[CrossRef](#)] [[PubMed](#)]
39. Bühl, M.; Wipff, G. Insights into Uranyl Chemistry from Molecular Dynamics Simulations. *ChemPhysChem* **2011**, *12*, 3095–3105. [[CrossRef](#)] [[PubMed](#)]
40. Frisch, G.A.; Trucks, M.J.; Schlegel, G.W.; Scuseria, H.B.; Robb, G.E.; Cheeseman, M.A.; Scalmani, J.R.; Barone, G.; Petersson, V. *Gaussian 16, Rev. C.01*; Gaussian, Inc.: Wallingford, CT, USA, 2016.
41. Weinhold, F.; Landis, C.; Glendening, E.D. What is NBO analysis and how is it useful? *Int. Rev. Phys. Chem.* **2016**, *35*, 399–440. [[CrossRef](#)]
42. Lu, T.; Chen, F. Multiwfn: A multifunctional wavefunction analyzer. *J. Comput. Chem.* **2012**, *33*, 580–592. [[CrossRef](#)] [[PubMed](#)]
43. Momma, K.; Izumi, F. VESTA: A three-dimensional visualization system for electronic and structural analysis. *J. Appl. Crystallogr.* **2008**, *41*, 653–658. [[CrossRef](#)]
44. Su, P.; Jiang, Z.; Chen, Z.; Wu, W. Energy decomposition scheme based on the generalized Kohn–Sham scheme. *J. Phys. Chem. A* **2014**, *118*, 2531–2542. [[CrossRef](#)] [[PubMed](#)]
45. Schmidt, M.W.; Baldridge, K.K.; Boatz, J.A.; Elbert, S.T.; Gordon, M.S.; Jensen, J.H.; Koseki, S.; Matsunaga, N.; Nguyen, K.A.; Su, S.; et al. General atomic and molecular electronic structure system. *J. Comput. Chem.* **1993**, *14*, 1347–1363. [[CrossRef](#)]
46. Stephens, P.J.; Devlin, F.J.; Chabalowski, C.F.; Frisch, M.J. Ab initio calculation of vibrational absorption and circular dichroism spectra using density functional force fields. *J. Phys. Chem.* **1994**, *98*, 11623–11627. [[CrossRef](#)]
47. Grimme, S.; Ehrlich, S.; Goerigk, L. Effect of the damping function in dispersion corrected density functional theory. *J. Comput. Chem.* **2011**, *32*, 1456–1465. [[CrossRef](#)] [[PubMed](#)]
48. Grimme, S.; Antony, J.; Ehrlich, S.; Krieg, H. A consistent and accurate ab initio parametrization of density functional dispersion correction (DFT-D) for the 94 elements H–Pu. *J. Chem. Phys.* **2010**, *132*, 154104. [[CrossRef](#)] [[PubMed](#)]
49. Kühne, T.D.; Iannuzzi, M.; Del Ben, M.; Rybkin, V.V.; Seewald, P.; Stein, F.; Laino, T.; Khaliullin, R.Z.; Schütt, O.; Schiffmann, F.; et al. CP2K: An electronic structure and molecular dynamics software package—Quickstep: Efficient and accurate electronic structure calculations. *J. Chem. Phys.* **2020**, *152*, 194103. [[CrossRef](#)] [[PubMed](#)]

Disclaimer/Publisher’s Note: The statements, opinions and data contained in all publications are solely those of the individual author(s) and contributor(s) and not of MDPI and/or the editor(s). MDPI and/or the editor(s) disclaim responsibility for any injury to people or property resulting from any ideas, methods, instructions or products referred to in the content.